Anisotropic spin relaxation in exchange-coupled ferromagnet/topological-insulator Fe/Bi$_2$Se$_3$ heterojunctions

Rui Sun [1,2,3] Yun-bin Sun,[4] Na Li,[1,2] Hao-Pu Xue,[1,2] Yan Li,[1,2] Xu Yang,[1,5] Yang Li,[1,2] Andrew H. Comstock,[3] Dali Sun [3] Wei He [1] Xiang-Qun Zhang,[1] and Zhao-Hua Cheng [1,2,5,*]

[1]*Beijing National Laboratory for Condensed Matter Physics, Institute of Physics, Chinese Academy of Sciences, Beijing 100190, China*
[2]*School of Physical Sciences, University of Chinese Academy of Sciences, Beijing 100049, China*
[3]*Organic and Carbon Electronics Lab (ORaCEL), Department of Physics, North Carolina State University, Raleigh, North Carolina 27695, USA*
[4]*Key Laboratory of Magnetism and Magnetic Materials at Universities of Inner Mongolia Autonomous Region, Department of Physics, Baotou Normal University, Baotou 014030, People's Republic of China*
[5]*Songshan Lake Materials Laboratory, Dongguan, Guangdong 523808, China*

The elegant spin physics of Dirac electrons in topological insulators (TIs) have considerably endowed fertile tunability of magnetic/TI heterojunction performance with modified spin-orbit effect engineering. Signatures of proximate hybridization between magnetic states and topological surface states have been reported. However, the nature of the spin relaxation process in these systems remains elusive. Here, we unambiguously demonstrate anisotropic spin relaxation in a spin-orbit-hybridized Fe/Bi$_2$Se$_3$ system. We find a sixfold anisotropy of the Gilbert damping parameter with modulation of up to 33% in Fe/Bi$_2$Se$_3$ in the presence of a topological surface state, together with a sixfold magnetic anisotropy. We anticipate the presence of a spin interplay between the topological spin-orbit texture and magnetic orbital states would manifest an anisotropic Gilbert damping, which corroborates with the density functional theory calculations. It is further demonstrated by the spin Hanle effect indicative of anisotropic spin relaxation time τ_s in the adjacent topological layer, inversely scaling with the Gilbert damping factor α_G. Our findings present an alternative scenario of the anisotropic spin transport process and offer insights into spin manipulation in spin-logic/memory devices utilizing proximity-hybridized Dirac electrons.

I. INTRODUCTION

Emergent two-dimensional Rashba and Dirac surface states possessing spin-momentum locking electrons have ignited an exotic bloom of spintronics [1–6]. The heterojunction of such novel states with magnetic materials leads to flourishing spin phenomena including spin-charge interconversion [7], a giant spin-pumping effect [8], large spin-orbit torque [9], unidirectional spin Hall magnetoresistance [10], etc. The spin of electrons accumulated at the interface is highly sensitive to the embedded interfacial states from the proximity effects or lower symmetry [11–13]. In particular, the transmission or spin-flip rate of pure spin current through the interface may be significantly modulated [14–17].

The Gilbert damping factor α_G is an essential dynamic parameter of the magnetic system to determine the power consumption and magnetic switching speed, which is sensitive to variations of interfacial properties, especially the spin-orbit coupling (SOC). Three-dimensional (3D) TIs with strong SOC can greatly modulate the spin dynamics of the magnetic layer by modifying the topological surface state (TSS) [18–20]. Additionally, the interplay of magnetic moment and

Dirac electrons of the TSS has given rise to the existence of exchange coupling and band structure hybridization at the interface and led to an enhanced α_G and modified magnetic anisotropy [21–23]. These experiments have suggested that exchange and spin-orbit coupling should influence the magnetization dynamics arising from the hybridized magnetic orbital states [24,25]. However, it remains elusive how the modification of the spin transmission and spin dissipation rate undergoes the action of spin-orbit interaction from the TSS.

Here, we found an exchange-coupled system, namely, a ferromagnet/topological-insulator bilayer (Fe/Bi$_2$Se$_3$) with an occurrence of a sixfold magnetic anisotropy when the TSS exists. Such a unique magnetic anisotropy from the interface is accompanied by a sixfold anisotropic Gilbert damping factor indicating the spin-related energy dissipation through the interface. In the previous report, an anisotropic Gilbert damping factor found in Fe/GaAs was ascribed to the interface-induced anisotropic electron band structures in Fe, i.e., anisotropic SOC and electron density of states $n(E_F)$ [26]. Considering a much thicker and polycrystalline Fe layer of a thickness of 11 nm in our system, the maximum-minimum damping ratio of up to 133% should be greatly smeared due to the random electron scattering in the presence of localized energy bands. Alternatively, we anticipate the anisotropic damping factor is tightly related to the anisotropic spin-flip scattering

*Contact author: zhcheng@iphy.ac.cn

024408-1
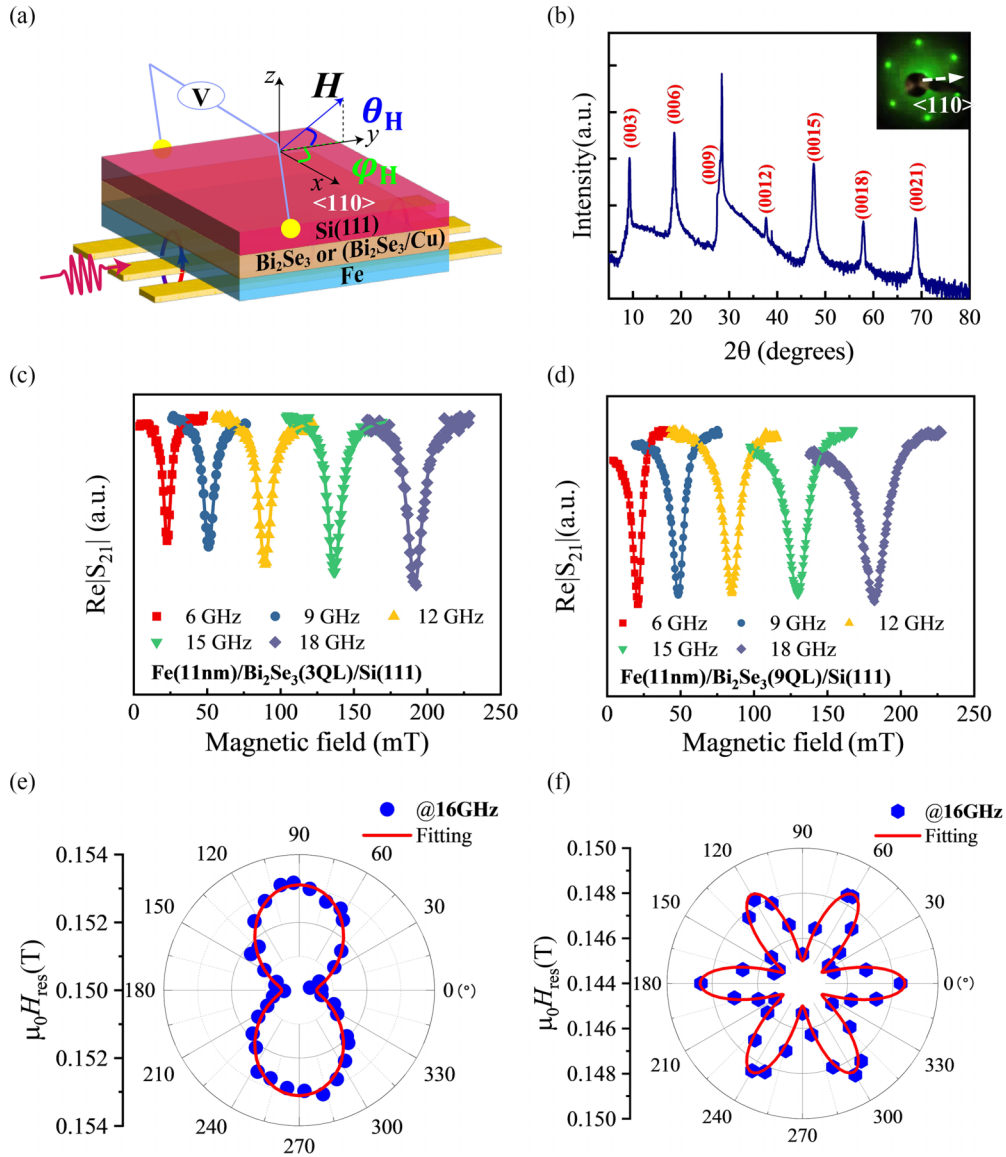
FIG. 1. (a) Schematic diagram of measurement configuration and defined coordinate system. (b) X-ray diffraction and low-energy electron diffraction pattern of 9-QL Bi_2Se_3 on Si(111). The arrow points to the $\langle 110 \rangle$ direction ($\Gamma - K$) of grown Bi_2Se_3, which is defined as the x axis. (c) and (d) Real part of S_{21} vs magnetic field at different frequencies for Fe(11 nm)/Bi_2Se_3(3 QL)/Si(111) (FBS-3) and Fe(11 nm)/Bi_2Se_3(9 QL)/Si(111) (FBS-9), respectively. (e) Resonance field H_{res}@16 GHz at different azimuthal φ_H for FBS-3 and FBS-9 (f), respectively. The solid lines are fitting curves.

rate of electrons from the interfacial exchange-coupled TSS in Bi_2Se_3. Based on the spin Hanle effect, we observed a magnetization-orientation-dependent spin relaxation time in Fe/Bi_2Se_3 where the spin component of the exchange-coupled TSS is correlated to the magnetization state and modulates the spin scattering process. The observation of the anisotropic damping factor and spin relaxation time in one system reveals the important role of the electron spin-flip rate of exchange-coupled conduction bands on the Gilbert damping factor in magnetic heterojunctions.

II. RESULTS

Bi_2Se_3 films with 3 and 9 quintuple layers (QLs; 1 QL = 0.95 nm) were thermally evaporated onto Si(111) substrate via the high-vacuum molecular beam epitaxy. Fe films with a thickness of 11 nm were deposited onto the Bi_2Se_3 surfaces at room temperature with a 2-nm Cu capping layer on top via e-beam evaporation. The high-quality single crystalline thin films Bi_2Se_3 are verified via x-ray diffraction exhibiting all (00*l*) diffraction peaks and six sharp low-energy electron diffraction spots, shown in Fig. 1(b). The large scale well-ordered Bi_2Se_3 surface provides a platform for the exploration of the regulated TSS effect exerted on the spin current transport.

The Cu(2 nm)/Fe(11 nm)/Bi_2Se_3(3 or 9 QL)/Si(111) samples (FBS-3 or FBS-9) were face-down mounted to the coplanar waveguide with applied magnetic field $\boldsymbol{H}$ along the azimuthal angle φ_H with respect to the x axis, i.e., the Bi_2Se_3 $\langle 110 \rangle$ direction; i.e., $\Gamma - K$ direction in reciprocal space. The

magnetic resonance is studied in the microwave frequency range from 6 to 20 GHz. Figures 1(c) and 1(d) depict typical Re$|S_{21}|$ spectra at several discrete frequencies with H along $\varphi_H = 0°$ for FBS-3 and FBS-9, respectively. The H-dependent resonance spectra Re$|S_{21}|$ at a fixed frequency f can be described by [27]

$$\text{Re } S_{21}(H) = a_1 + b_1 \frac{\Delta H^2}{(H - H_{\text{res}})^2 + \Delta H^2}$$
$$+ b_2 \frac{\Delta H(H - H_{\text{res}})}{(H - H_{\text{res}})^2 + \Delta H^2}, \quad (1)$$

where H_{res} is the resonance field and ΔH is the half width at half maximum linewidth at resonance frequency f. The linewidth ΔH for FBS-9 with TSS is broader than that for FBS-3 without TSS while the difference in the resonance field H_{res} between the two samples is moderate. According to the Landau-Lifshitz-Gilbert equation in the spin current transport regime, the dissipation of spin current ejecting from the magnetic system will lead to an enhancement of the intrinsic Gilbert damping factor. The obvious linewidth broadening in FBS-9 indicates a distinct role of the TSS in spin current transmission compared to the FBS-3 sample. Next, we performed azimuthal angle φ-dependent measurements from $0°$ to $360°$. The angular dependence of H_{res} at 16 GHz for FBS-3 and FBS-9 is quite distinct, as shown in Figs. 1(e) and 1(f). The FBS-3 sample exhibits a uniaxial magnetic anisotropy while the FBS-9 sample indicates a sixfold magnetic anisotropy. To describe the magnetic system, the free energy of magnetization can be written as [28]

$$E = -\mu_0 M_s \boldsymbol{H} \cdot \boldsymbol{\mu} + \frac{1}{2}\mu_0 M_s^2$$
$$+ 2H_1 M_s\left(\alpha_1^2\alpha_2^2 + \alpha_2^2\alpha_3^2 + \alpha_3^2\alpha_1^2\right) + 2H_2 M_s\left(\alpha_1^2\alpha_2^2\alpha_3^2\right)$$
$$- 2H_u M_s(\boldsymbol{\mu} \cdot \boldsymbol{n_u})^2 - 2H_s M_s(\boldsymbol{\mu} \cdot \boldsymbol{n_s})^2, \quad (2)$$

where α_i ($i = 1, 2, 3$) represents the directional cosines of the magnetic unit vector $\boldsymbol{\mu}$ with respect to the cubic coordinate axes [100], [010], and [001]. μ_0 is the vacuum permutability; M_s is the saturation magnetization of Fe; and H_1, H_2, H_u, and H_s are fourfold, sixfold, uniaxial, and interfacial anisotropy fields, respectively. The unit vectors $\boldsymbol{n_u}$ and $\boldsymbol{n_s}$ point along the direction of the easy axis of the uniaxial magnetic anisotropy and normal to the film plane. Combined with the standard ferromagnetic resonance (FMR) conditions [28], it is found that FBS-3 yields an $H_u \sim 7$ mT while H_u is absent in FBS-9 although it possesses a comparable magnetic anisotropy field strength of a sixfold anisotropy $H_2 \sim 5.7$ mT. The origin of such a magnetic anisotropy difference is intricate. The uniaxial magnetic anisotropy for the FBS-3 is likely originated from the growth mainly influenced by the morphology while the sixfold magnetic anisotropy H_2 for the FBS-9 possibly stems from the interface but is not induced by the magnetocrystalline anisotropy due to the nonepitaxial growth of Fe on Bi_2Se_3. For the epitaxial Fe thin film on Si, its magnetic anisotropies are dominated by the H_u, superimposed with magnetocrystalline anisotropies H_1 and H_2 (see Fig. S2 in the Supplemental Material [29]).

Since Gilbert damping of the system directly reflects information of the spin current transmission and is sensitive to

the variation of spin-orbit interaction [22,26], the angular and frequency dependence of the linewidth was extracted for each sample to study this relationship. Figure 2(a) depicts several typical ΔH vs f curves along the easy axis (EA) and hard axis (HA) of the magnetic system, respectively. The relationship can be written as [32]

$$\mu_0\Delta H = \mu_0\Delta H_0 + \frac{2\pi\alpha_G}{\gamma}f, \quad (3)$$

where $\mu_0\Delta H_0$ is the inhomogeneous broadening due to disorder, γ is the gyromagnetic ratio of Fe (184 GHz/T), and α_G is the Gilbert damping factor. The α_G of FBS-9 determined by the slope in Fig. 2(a) varies along the EA and HA directions. The fitted values of α_G for FBS-9 are about 0.0115 ($\pm$0.0001) along the EA direction and 0.0153 ($\pm$0.0001) along the HA direction. The quite small magnetocrystalline anisotropy field indicates the contribution from the mosaicity effect, and the field-drag effect could be very small [33–35]. In terms of the two-magnon scattering, it can lead to an additional linewidth broadening term,

$$\Delta H_{2M} = \Gamma\sin^{-1}\sqrt{\frac{\sqrt{(2\pi f)^2 + \left(\frac{2\pi f_0}{2}\right)^2} - \left(\frac{2\pi f_0}{2}\right)}{\sqrt{(2\pi f)^2 + \left(\frac{2\pi f_0}{2}\right)^2} + \left(\frac{2\pi f_0}{2}\right)}}\Bigg/2, \quad (4)$$

where $f_0 = \frac{\gamma\mu_0}{2\pi}M_{\text{eff}}$, which could mislead to an extrinsic damping factor anisotropy. After adding a two-magnon scattering term into the damping factor fit process, the anisotropy of the damping factor for FBS-9 does not change, which implies that the contribution of two-magnon scattering to the Gilbert damping factor anisotropy could be negligible (see details in Fig. S4 [29]). As plotted in Fig. 2(d), the α_G of FBS-9 exhibits sixfold symmetry in the same way as its magnetic anisotropy does. Compared to the FBS-9 sample, the slope of ΔH vs f for FBS-3 along the EA, HA, and other directions are almost identical in Fig. 2(b). Exploiting Eq. (3), the α_G of FBS-3 in Fig. 2(e) shows an isotropic feature with a value of $\alpha_G \sim 0.0133 \pm 0.0001$ slightly smaller than the maximum α_G of FBS-9. The Gilbert damping factor can be decomposed into two parts, $\alpha_G = \alpha_{\text{Fe}} + \Delta\alpha$. α_{Fe} is the intrinsic damping factor of Fe about 0.0055 ± 0.0001 that is isotropic on Si(111) substrate (see Fig. S2 [29]). The additional damping factor $\Delta\alpha$ in the heterostructure commonly originates from the spin-pumping effect or the interfacial exchange-coupled effects reported in magnetic/heavy metal systems such as Co/Pt [36]. Thus, a 2-nm Cu layer was inserted between the Fe and Bi_2Se_3 layer to space the possible coupling. Figure 2(c) shows the relationship between ΔH vs f at various angles for Fe/Cu/Bi_2Se_3 (FCBS-9). Despite the moderate changes in intercept ΔH_0, the Gilbert damping α_G of FCBS-9 is isotropic, similar to FBS-3. The isotropic Gilbert damping is about 0.0096 ± 0.0001, comparable to the minimum of FBS-9 depicted in Fig. 2(f). In a FM$_1$/nonmagnet/FM$_2$ bilayer system, the relative orientation of these two magnetic states can affect the damping factor via the anisotropic spin backflow process where the spin backflow will be maximized when magnetization $\mathbf{m}_1$ in FM1 is parallel to $\mathbf{m}_2$ in FM2. However, this process cannot be actively present due to the single ferromagnetic state in our case.
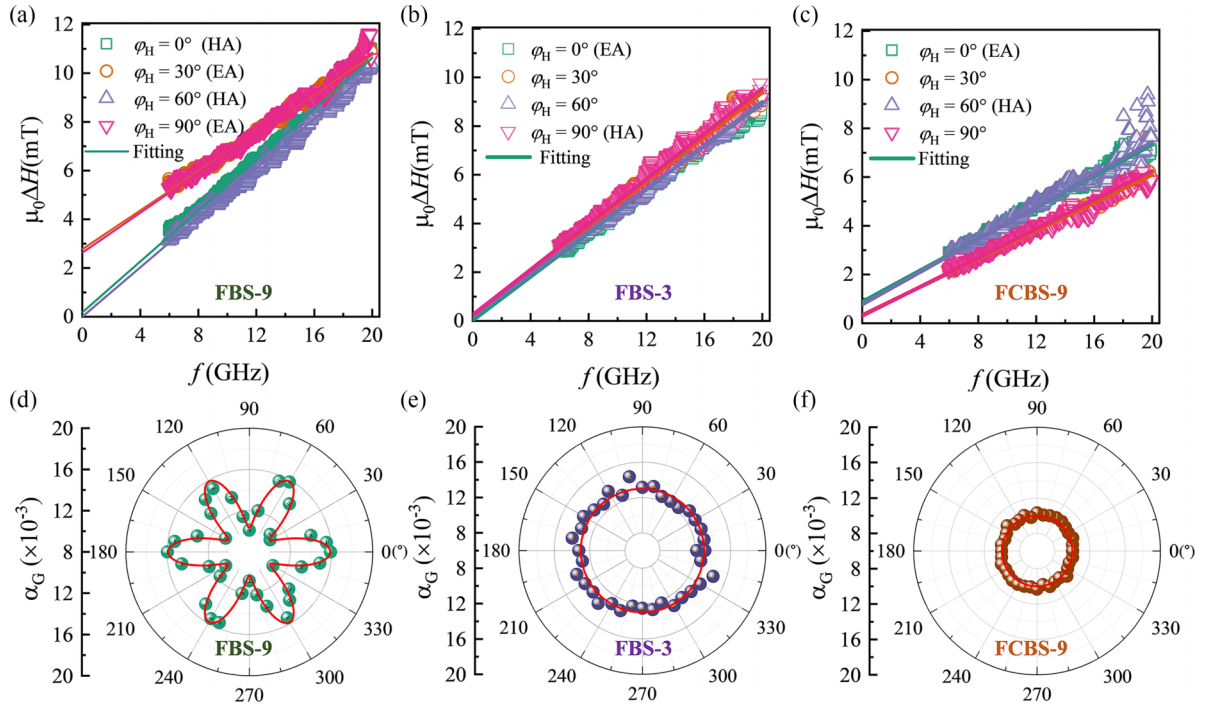
FIG. 2. Top panel: (a)–(c) Resonance linewidth ΔH vs frequency f along the separate azimuthal direction with $\varphi_H = 0°, 30°, 60°, 90°$ for FBS-9, FBS-3, and FCBS-9 samples. EA and HA represent the easy and hard axes of magnetic anisotropy. The green, yellow, purple, and pink solid lines are fitting curves. Bottom panel: (d)–(f) The obtained value of Gilbert damping factor α vs azimuthal φ_H. The red solid lines are a guide for the eyes.

While in terms of the anisotropy of the Gilbert damping, previously reported in an epitaxial Fe/GaAs system, the anisotropic interfacial SOC leads to a twofold density of states and therefore a uniaxial damping factor anisotropy in the Fe layer with a thickness less than 1.3 nm [26]. For the FBS-9 with an 11-nm Fe layer, while the topological surface state will be preserved with a thickness above 5 QL [22,37], it is much less likely that the origin of the anisotropic damping factor is the anisotropic density of states in the magnetic layer induced by the hexagonally wrapped spin-orbit texture of the Bi_2Se_3 layer. The larger thickness of the Fe layer will weaken the magnitude of the SOC proximity effect in the Fe layer. On the other hand, with a 2-nm Cu layer spaced between Fe and 9-QL Bi_2Se_3, the anisotropy of the Gilbert damping factor would fade away despite the presence of a proximate warped spin-orbit field of Bi_2Se_3 interfaced with Cu [38]. Therefore, it implies that the disappearance of the damping anisotropy via the Cu spacer layer rules out an anisotropic spin-pumping effect from the isolated TSS itself. It further indicates the exchange coupling or proximity effect between Fe orbitals and the TSS does play a dominant role, resulting in an unexpected anisotropy of the Gilbert damping factor with a distinguished physical origin compared to the quintessential Fe/GaAs heterostructure. In the previous study of the anisotropic damping factor, interfacial SOC and density of states of the magnetic layer were considered as the origin of the anisotropic Gilbert damping factor [26,39]. On the other hand, the spin relaxation time of the adjacent layer, which is a crucial factor in determining the spin current transport and is tightly related to the Gilbert damping factor, yet, is overlooked in the FMR-type

damping factor measurement where the dissipation of spin current occurring through or in the topological interface will modify the damping factor in general.

To buttress the relationship between the Gilbert damping factor α_G and spin relaxation time τ_s, oblique Hanle effect measurements were conducted for FBS-3, FBS-9, and FCBS-9 along the HA and EA directions, respectively. The inset of Fig. 3(a) depicts the schematic setup based on spin-pumping voltage detection. Under microwave excitation, spin current is injected into the adjacent Bi_2Se_3 layer. Due to the inverse Edelstein effect (IEE) [40], the spin current is converted into a detectable transverse spin-pumping voltage V_{sp}. When the magnetic field H is applied along an out-of-plane angle θ_H, the magnetization precession axis is not aligned along H due to the demagnetization field. The injected spin current with spin polarization S along the magnetization precession axis will diffuse into the Bi_2Se_3 layer and precess about H with a decaying amplitude governed by the spin relaxation time τ_s. This Hanle-type precession of S will alter the magnitude of the spin current density, and result in a voltage response $V_{IEE}(\theta_H)$ deviating from $V_{IEE} \propto \cos\theta_M$ angular dependence to a more gradual manifestation [41]. This can be described in the Bloch equation with spin diffusion and precession [41]:

$$\frac{\partial S(z,t)}{\partial t} = \gamma_c[S(z,t) \times H] - \frac{S(z,t)}{\tau_s} + D_N \nabla^2 S(z,t)$$
$$+ 2\left(J_{s,z}^z e_z + J_{s,z}^y e_y\right)\delta(z), \tag{5}$$

where γ_c and τ_s are the gyromagnetic ratio and spin relaxation time of the carrier in Bi_2Se_3. D_N is the spin diffusion constant
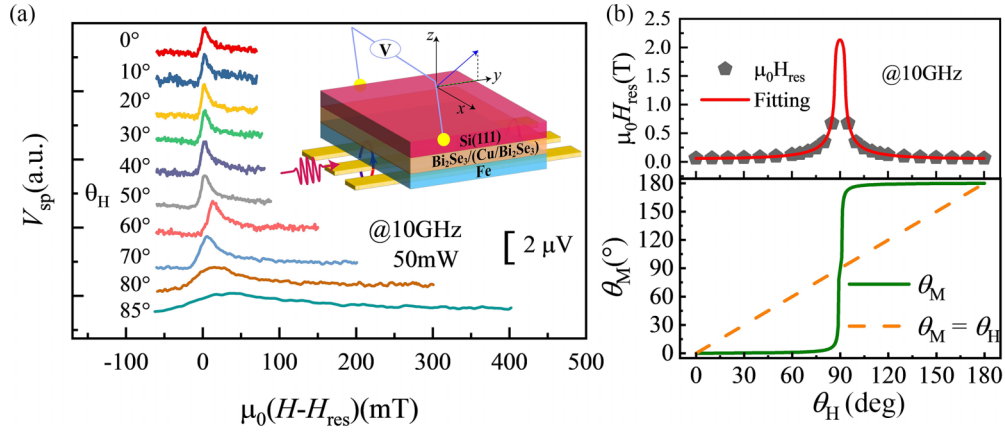
FIG. 3. (a) Typical spin-pumping voltage response V_{sp} as a function of the magnetic field. The colorful curves are experimental raw data at different θ_H from $0°$ to $85°$. The microwave is fixed at 10 GHz with a power of 50 mW. The inset shows the schematic image of the measurement configuration. (b) The experimental resonance field H_{res} vs θ_H at 10 GHz (top panel). The red solid line is the simulated curve. The calculated magnetization angle θ_M vs θ_H is shown in the bottom panel.

and $J_{s,j}^{i}$ is the spin current density with spin direction i and propagates along direction $j(i, j = x, y, z)$. e_y and e_z are the unit vectors along the y and z axes and $\delta(z)$ is the delta function.

Figure 3(a) shows the θ_H dependence of the V_{sp} response as a function of magnetic field H at a fixed frequency $f = 10$ GHz for FBS-9. The V_{sp} response can be decomposed into a symmetric and an antisymmetric part, namely, $V_{sp} = V_s \frac{\Delta H^2}{(H-H_{res})^2+\Delta H^2} + V_a \frac{\Delta H(H-H_{res})}{(H-H_{res})^2+\Delta H^2}$, where V_s mainly comes from the IEE process while V_a is dominated by the side effects from anisotropic magnetoresistance and anomalous Hall effect [42]. Evidently, V_s diminishes at a high angle under the Hanle spin precession. The relation of measured resonance field H_{res} as a function of θ_H is simulated in Fig. 3(b) and the magnetization angle θ_M vs θ_H is also obtained in Fig. 3(b) (bottom panel) according to standard FMR conditions [43].

To minimize the influence of the thermal effects, the θ_H dependence of the spin-charge conversion component V_{IEE} is calculated via $V_{IEE} = [V_s(+H) - V_s(-H)]/2$. Figure 4 shows the observed angular dependence of V_{IEE} in different devices for various in-plane directions, i.e., the EA and HA of each sample. The angular dependence of V_{IEE} in the presence of Hanle precession can be expressed as [41,44,45]

$$V_{IEE}(\theta_H) \propto J_s \left(\cos\theta_H \cos(\theta_H - \theta_M) \int_0^{d_N} e^{-x/\lambda_N} dx \right.$$
$$\left. + \sin\theta_H \sin(\theta_H - \theta_M) \int_0^{d_N} \mathrm{Re}[e^{-x/\lambda_\omega}] dx \right),$$
$$(6)$$

where d_N is the effective thickness of the spin-charge conversion layer of Bi_2Se_3 and λ_N is the effective spin diffusion length; $\lambda_\omega = \lambda_N/\sqrt{1+i\omega_L\tau_s}$ and $\omega_L = \gamma_c H_{res}$ (γ_c is the gyromagnetic ratio of the electron); and J_s is the spin current density injected into the Bi_2Se_3 at each θ_H. Since Bi_2Se_3 possesses very strong SOC strength and V_{IEE} is converted by the topological surface states of Bi_2Se_3, we assume the

$d_N = \lambda_N = 1$ QL for simplified analysis [45]. For the FBS-9 sample, we found the normalized $V_{IEE}(\theta_H)$ along the EA direction is more gradual than along the HA direction. The experimental data for both directions can be well produced via Eq. (6), yielding the value of spin relaxation time $\tau_s = 70 \pm 5$ ps (EA) and $\tau_s = 10 \pm 5$ ps (HA), respectively. The anisotropy in spin relaxation time serves as direct evidence of anisotropic spin current transport modulated by hybridization between Fe and the TSS. By measuring the Hanle spin precession for samples FBS-3 and FCBS-9, the τ_s is almost identical along both EA and HA directions without exhibiting any anisotropy of spin relaxation time. The estimation of τ_s for FBS-3 is about 30 ± 5 ps, a little shorter than FCBS-9 with $\tau_s \sim 70 \pm 5$ ps. Due to the suppression of backscattering from the spin-momentum-locked TSS, the spin relaxation time τ_s in FCBS-9 may be prolonged despite its strong intrinsic SOC strength [45]. Thus, it is reasonable the FCBS-9 possesses a longer τ_s with the TSS. For the FBS-9 where the TSS is preserved in the presence of hybridization [25], spin scattering may be enhanced along the HA due to hybridized electron states leading to a reduction of τ_s to 10 ps, while a larger τ_s of 70 ps remains along the EA. The different spin relaxation time in the FBS-9 sample implies anisotropic spin scattering in the situation of the electron hybridization between Fe orbitals and the TSS.

Comprehensively examining the results obtained from FMR and spin Hanle measurements, we found the damping factor α_G and spin relaxation time τ_s corroborate each other. The anisotropic damping factor via FMR coexists with the anisotropic spin relaxation time revealed by the oblique Hanle precession measurement. The spin current transport process is identical where the spin current was injected, diffused, and finally dissipated in the Bi_2Se_3 layer via spin pumping. The anisotropic damping factor manifests itself in changes of the Gilbert damping factor while the spin lifetime evolves with modulating the spin-to-charge voltage due to Hanle precession. Each technique shows the anisotropic spin transport only occurs in the exchange-coupled FBS-9 system while the other two reveal isotropic spin properties. On the other
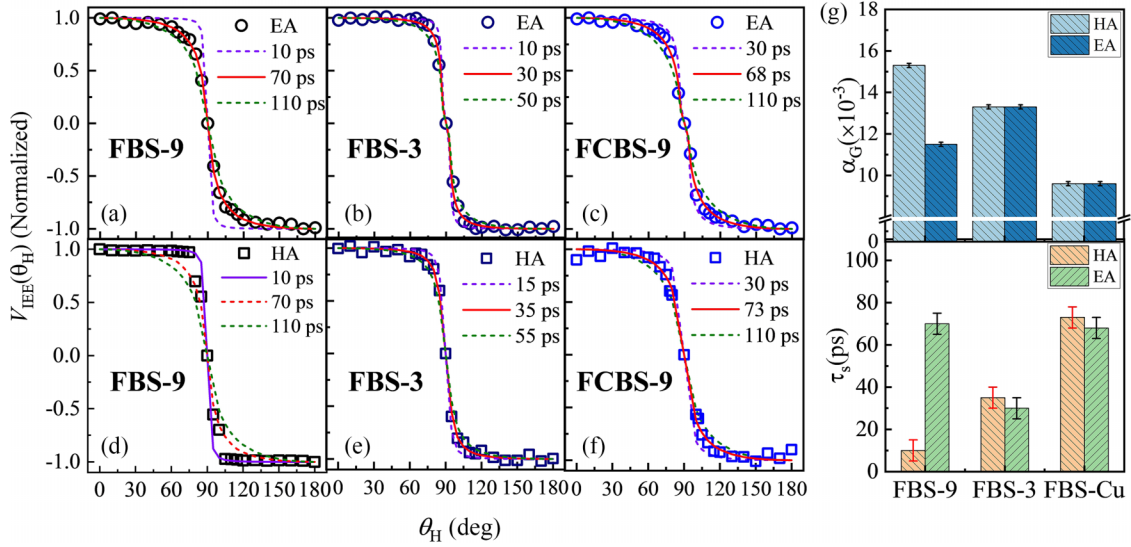
FIG. 4. The θ_H dependence of spin-to-charge conversion voltage $V_{IEE}(\theta_H)$ for FBS-9, FBS-3, and FCBS-9 along the EA direction (a)–(c) and along the HA direction (d)–(f), respectively. The solid lines are best-fitted curves. The dashed lines are plotted for comparison. (g) Comparison of Gilbert damping factor and spin relaxation time for FBS-9, FBS-3, and FCBS-9 along the EA and HA directions.

hand, the Gilbert damping factor α_G inversely scales with the spin relaxation time τ_s. Along the direction with the shortest $\tau_s = 10$ ps (FBS-9, HA), α_G is the largest (~ 0.0153). For α_G along the direction with τ_s about 70 ps in the EA direction of both FBS-9 and FCBS-9, α_G exhibits a similar value close to 0.01. Additionally, in the FBS-3 system, the spin relaxation time τ_s is 30 ps and its Gilbert damping factor $\alpha_G \sim 0.0133$, which is intermediate between FBS-9 HA and FCBS-9. It is well known that the enhancement of the Gilbert damping factor in multilayer systems can be generally attributed to the spin current dissipation via SOC. The dynamic spin current pumped from the Fe layer would be injected into the SOC layer, and relaxation occurs via SOC-type spin scattering. Phenomenologically, an additional damping factor $\Delta\alpha$ is proportional to the dissipation of spin current S, and such a process is governed by the spin-flip process, namely, leading

to $\Delta\alpha \propto (\frac{dS}{dt})_{sf} \propto \frac{S}{\tau_s}$ [46]. The intimate relationship between the anisotropic damping factor and spin relaxation time indicates the key role of spin flips in the dynamic spin transport process. Such a relationship can also preclude the dominant origin of anisotropic spin transport from the spin memory loss while the spin memory loss induced by the interfacial SOC can lead to an additional damping factor [47]. However, the lost spin current is a partial depolarization process via the spin flip, which cannot be converted into a charge current via IEE [48]. On the contrary, the spin lifetime obtained by the spin Hanle effect based on the spin-pumping measurements results from the electron spins involved with the IEE process.

The spin relaxation can come from spin-phonon interaction, hyperfine interaction, spin-orbit coupling, etc. Since there is spin-momentum locking from the TSS, the spin
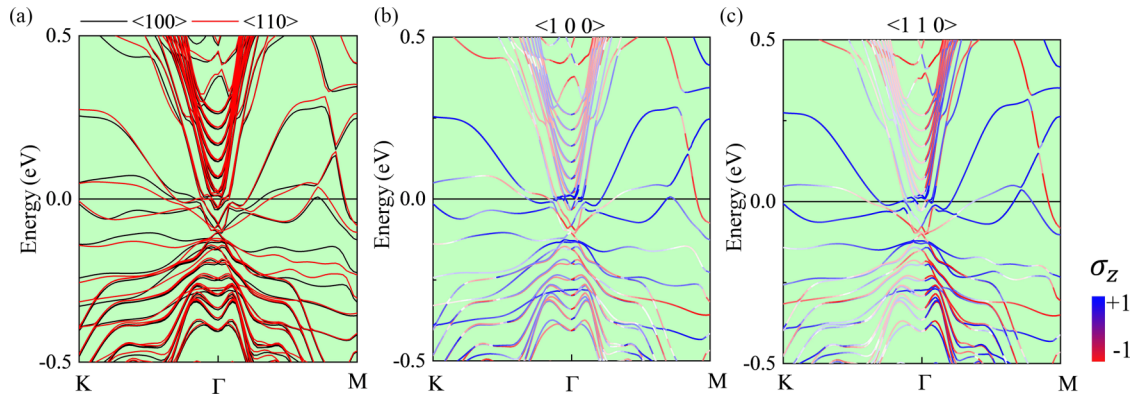
FIG. 5. Comparison of the band structure of Fe(6 ML)/Bi$_2$Se$_3$(9 QL) and spin polarization σ_z component distribution along Γ-K and Γ-M. (a) Overall energy band of Fe-Bi$_2$Se$_3$ when magnetization is along Γ-M (red curve, $\langle 100 \rangle$ direction) and Γ-K (black curve, $\langle 110 \rangle$ direction). Spin polarization σ_z component distribution near Fermi level when magnetization of Fe is along $\langle 100 \rangle$ (b) and $\langle 110 \rangle$ (c), respectively. The color of the right side (Γ-M) in (c) is much darker than that in (b) (Γ-K) near Fermi level, indicating the modulation of the σ_z component when alternating the magnetization. The blue and red colors depict the relative magnitude of the σ_z component.

relaxation process could likely be dominated by the SOC. The spin texture from the TSS, i.e., the spin-orbit field, would behave like an emergent effective magnetic field, giving rise to additional spin precession around the field direction or spin locking along the field direction in a spin-propagating media with spin-orbit field [49]. Moreover, the band deviation due to the alternation of magnetization direction could also lead to the anisotropy of spin interband and intraband scattering [50,51]. We performed the density functional theory (DFT) calculation on the Fe(6 ML)/Bi$_2$Se$_3$(9 QL) shown in Fig. 5(a). The details of energy bands from Bi$_2$Se$_3$ are barely changed near the Γ point although the Fe orbital states exhibit an energy band shift away from the exchange-coupled bands. It further implies it is less likely that the damping factor anisotropy comes from spin-orientation band structure changes such as the electron density state. However, there is a large difference in the σ_z component of spin texture when the magnetization is along Γ-K and Γ-M as depicted in Figs. 5(b) and 5(c). When the σ_z component is negligible with magnetization along $\langle 100 \rangle$, the spin relaxation time is longer likely due to the spin-locking property of the topological state depressing the spin precession. On the other hand, when the magnetization direction points to $\langle 110 \rangle$, the σ_z component becomes larger leading to the additional spin precession over the Fermi surface. On the contrary, the difference of the σ_z component is quite small in Fe(6 ML)/Bi$_2$Se$_3$(3 QL) (shown in Fig. S5 [29]) and there is none of the anisotropy of damping factor and spin relaxation time.

In conclusion, we observed a sixfold anisotropy of Gilbert damping in the exchange-coupled ferromagnet/topological-insulator (FM/TI) heterostructure. We also revealed such an anisotropic Gilbert damping factor phenomenon favorably originating from the orientation-dependent spin-flip process, which exhibits anisotropic spin relaxation time in the adjacent SOC layer. Since the swapping effect of magnetic exchange and spin-orbit coupling are ubiquitous in FM/TI, FM/heavy metal, and even a two-dimensional ferromagnetic/nonmagnetic material junction, we expect such an effect at the interface will exert a non-negligible role on spin transmission and spin relaxation, likely correlated to the magnetization-dependent spin texture revealed by DFT calculation. Our results also hint that there is a great likelihood of manufacturing more anisotropic spin/electronic systems utilizing the exchange-coupled proximity effect for functional applications.

All data needed to evaluate the conclusions in the paper are present in the paper and/or the Supplemental Material [29].

ACKNOWLEDGMENT

The authors declare that they have no competing interests.

[1] S. Manipatruni, D. E. Nikonov, and I. A. Young, Beyond CMOS computing with spin and polarization, Nat. Phys. **14**, 338 (2018).

[2] S. Manipatruni, D. E. Nikonov, C. C. Lin, T. A. Gosavi, H. Liu, B. Prasad, Y. L. Huang, E. Bonturim, R. Ramesh, and I. A. Young, Scalable energy-efficient magnetoelectric spin-orbit logic, Nature (London) **565**, 35 (2019).

[3] Y. Fan, P. Upadhyaya, X. Kou, M. Lang, S. Takei, Z. Wang, J. Tang, L. He, L.-T. Chang, M. Montazeri *et al.*, Magnetization switching through giant spin–orbit torque in a magnetically doped topological insulator heterostructure, Nat. Mater. **13**, 699 (2014).

[4] X. Wang, L. Cheng, D. Zhu, Y. Wu, M. Chen, Y. Wang, D. Zhao, C. B. Boothroyd, Y. M. Lam, J. X. Zhu *et al.*, Ultrafast spin-to-charge conversion at the surface of topological insulator thin films, Adv. Mater. **30**, e1802356 (2018).

[5] X. Lin, W. Yang, K. L. Wang, and W. Zhao, Two-dimensional spintronics for low-power electronics, Nat. Electron. **2**, 274 (2019).

[6] Y. Otani, M. Shiraishi, A. Oiwa, E. Saitoh, and S. Murakami, Spin conversion on the nanoscale, Nat. Phys. **13**, 829 (2017).

[7] W. Han, Y. Otani, and S. Maekawa, Quantum materials for spin and charge conversion, npj Quantum Mater. **3**, 27 (2018).

[8] M. Jamali, J. S. Lee, J. S. Jeong, F. Mahfouzi, Y. Lv, Z. Zhao, B. K. Nikolić, K. A. Mkhoyan, N. Samarth, and J.-P. Wang, Giant spin pumping and inverse spin Hall effect in the presence of surface and bulk spin−orbit coupling of topological insulator Bi$_2$Se$_3$, Nano Lett. **15**, 7126 (2015).

[9] A. R. Mellnik, J. S. Lee, A. Richardella, J. L. Grab, P. J. Mintun, M. H. Fischer, A. Vaezi, A. Manchon, E. A. Kim, N. Samarth *et al.*, Spin-transfer torque generated by a topological insulator, Nature (London) **511**, 449 (2014).

[10] Y. Lv, J. Kally, D. Zhang, J. S. Lee, M. Jamali, N. Samarth, and J.-P. Wang, Unidirectional spin-Hall and Rashba−Edelstein magnetoresistance in topological insulator-ferromagnet layer heterostructures, Nat. Commun. **9**, 111 (2018).

[11] S. Shi, A. Wang, Y. Wang, R. Ramaswamy, L. Shen, J. Moon, D. Zhu, J. Yu, S. Oh, Y. Feng *et al.*, Efficient charge-spin conversion and magnetization switching through the Rashba effect at topological-insulator/Ag interfaces, Phys. Rev. B **97**, 041115(R) (2018).

[12] R. Sun, S. Yang, X. Yang, E. Vetter, D. Sun, N. Li, L. Su, Y. Li, Y. Li, Z. Z. Gong *et al.*, Large tunable spin-to-charge conversion induced by hybrid Rashba and Dirac surface states in topological insulator heterostructures, Nano Lett. **19**, 4420 (2019).

[13] D. Khokhriakov, A. W. Cummings, K. Song, M. Vila, B. Karpiak, A. Dankert, S. Roche, and S. P. Dash, Tailoring emergent spin phenomena in Dirac material heterostructures, Sci. Adv. **4**, aat9349 (2018).

[14] M. Milletari, M. Offidani, A. Ferreira, and R. Raimondi, Covariant conservation laws and the spin Hall effect in Dirac-Rashba systems, Phys. Rev. Lett. **119**, 246801 (2017).

[15] R. Dey, N. Prasad, L. F. Register, and S. K. Banerjee, Conversion of spin current into charge current in a topological insulator: Role of the interface, Phys. Rev. B **97**, 174406 (2018).

[16] A. G. Moghaddam, A. Qaiumzadeh, A. Dyrdal, and J. Berakdar, Highly tunable spin-orbit torque and anisotropic magnetore-

sistance in a topological insulator thin film attached to ferromagnetic layer, Phys. Rev. Lett. **125**, 196801 (2020).

[17] L. Cheng, X. Wang, W. Yang, J. Chai, M. Yang, M. Chen, Y. Wu, X. Chen, D. Chi, K. E. J. Goh *et al.*, Far out-of-equilibrium spin populations trigger giant spin injection into atomically thin MoS$_2$, Nat. Phys. **15**, 347 (2019).

[18] Y. T. Fanchiang, K. H. M. Chen, C. C. Tseng, C. C. Chen, C. K. Cheng, S. R. Yang, C. N. Wu, S. F. Lee, M. Hong, and J. Kwo, Strongly exchange-coupled and surface-state-modulated magnetization dynamics in Bi$_2$Se$_3$/yttrium iron garnet heterostructures, Nat. Commun. **9**, 223 (2018).

[19] C. Tang, Q. Song, C. Z. Chang, Y. D. Xu, Y. Ohnuma, M. Matsuo, Y. W. Liu, W. Yuan, Y. Y. Yao, J. S. Moodera *et al.*, Dirac surface state-modulated spin dynamics in a ferrimagnetic insulator at room temperature, Sci. Adv. **4**, aas8660 (2018).

[20] K. Kondou, R. Yoshimi, A. Tsukazaki, Y. Fukuma, J. Matsuno, K. S. Takahashi, M. Kawasaki, Y. Tokura, and Y. Otani, Fermi-level-dependent charge-to-spin current conversion by Dirac surface states of topological insulators, Nat. Phys. **12**, 1027 (2016).

[21] G. Wu, D. Wu, Y. Ren, Q. Y. Jin, and Z. Zhang, Topological surface state manipulation of magnetic damping and surface anisotropy in topological insulator/nonmagnet/CoFe heterostructures, Phys. Rev. B **103**, 014419 (2021).

[22] N. Li, Y.-B. Sun, R. Sun, X. Yang, W. Zhang, Z.-K. Xie, J.-N. Liu, Y. Li, Y. Li, Z.-Z. Gong *et al.*, Topological surface state enhanced ultrafast spin dynamics of Fe/Bi$_2$Se$_3$ heterostructures, Phys. Rev. B **105**, 144415 (2022).

[23] X. Zhang, C. H. Li, J. Moon, S. Leontsev, M. R. Page, B. T. Jonker, and O. van 't Erve, Interplay of spin current and magnetization in a topological-insulator/magnetic-insulator bilayer structure, Phys. Rev. Mater. **6**, 074203 (2022).

[24] P. Rüßmann, S. K. Mahatha, P. Sessi, M. A. Valbuena, T. Bathon, K. Fauth, S. Godey, A. Mugarza, K. A. Kokh, O. E. Tereshchenko *et al.*, Towards microscopic control of the magnetic exchange coupling at the surface of a topological insulator, J. Phys. Mater. **1**, 015002 (2018).

[25] Y. S. Hou and R. Q. Wu, Strongly enhanced Gilbert damping in 3*d* transition-metal ferromagnet monolayers in contact with the topological insulator Bi$_2$Se$_3$, Phys. Rev. Appl. **11**, 054032 (2019).

[26] L. Chen, S. Mankovsky, S. Wimmer, M. A. W. Schoen, H. S. Körner, M. Kronseder, D. Schuh, D. Bougeard, H. Ebert, D. Weiss *et al.*, Emergence of anisotropic Gilbert damping in ultrathin Fe layers on GaAs(001), Nat. Phys. **14**, 490 (2018).

[27] Y. Li, Y. Li, R. Sun, N. Li, Z.-Z. Gong, X. Yang, Z.-K. Xie, H.-L. Liu, W. He, X.-Q. Zhang *et al.*, Anomalous Gilbert damping induced by the coexisting static and dynamic coupling in Fe/Pd/Fe trilayers, Phys. Rev. B **104**, 094409 (2021).

[28] S. M. Rezende, J. A. S. Moura, F. M. de Aguiar, and W. H. Schreiner, Ferromagnetic resonance of Fe(111) thin films and Fe(111)/Cu(111) multilayers, Phys. Rev. B **49**, 15105 (1994).

[29] See Supplemental Material at http://link.aps.org/supplemental/10.1103/PhysRevB.110.024408 for thin film characterization with low-energy electron diffraction; magnetization dynamics of expitaxial Fe on Si(111); contribution of two-magnon scattering in FBS-9; and details of the Hanle model to obtain the spin relaxation time and Fe(6 ML)/Bi$_2$Se$_3$(3 QL). The Supplemental Material also contains Refs. [30,31].

[30] K. Lenz, H. Wende, W. Kuch, K. Baberschke, K. Nagy, and A. Jánossy, Two-magnon scattering and viscous Gilbert damping in ultrathin ferromagnets, Phys. Rev. B **73**, 144424 (2006).

[31] L. Chen, S. Mankovsky, M. Kronseder, D. Schuh, M. Prager, D. Bougeard, H. Ebert, D. Weiss, and C. H. Back, Interfacial tuning of anisotropic Gilbert damping, Phys. Rev. Lett. **130**, 046704 (2023).

[32] J. O. Rantschler, R. D. McMichael, A. Castillo, A. J. Shapiro, W. F. Egelhoff, B. B. Maranville, D. Pulugurtha, A. P. Chen, and L. M. Connors, Effect of 3*d*, 4d, and 5*d* transition metal doping on damping in permalloy thin films, J. Appl. Phys. **101**, 033911 (2007).

[33] K. Zakeri, J. Lindner, I. Barsukov, R. Meckenstock, M. Farle, U. von Hörsten, H. Wende, W. Keune, J. Rocker, S. S. Kalarickal *et al.*, Spin dynamics in ferromagnets: Gilbert damping and two-magnon scattering, Phys. Rev. B **76**, 104416 (2007).

[34] R. D. McMichael, D. J. Twisselmann, and A. Kunz, Localized ferromagnetic resonance in inhomogeneous thin films, Phys. Rev. Lett. **90**, 227601 (2003).

[35] L. Chen, M. Decker, M. Kronseder, R. Islinger, M. Gmitra, D. Schuh, D. Bougeard, J. Fabian, D. Weiss, and C. H. Back, Robust spin-orbit torque and spin-galvanic effect at the Fe/GaAs (001) interface at room temperature, Nat. Commun. **7**, 13802 (2016).

[36] S. Azzawi, A. Ganguly, M. Tokaç, R. M. Rowan-Robinson, J. Sinha, A. T. Hindmarch, A. Barman, and D. Atkinson, Evolution of damping in ferromagnetic/nonmagnetic thin film bilayers as a function of nonmagnetic layer thickness, Phys. Rev. B **93**, 054402 (2016).

[37] Y. Zhang, K. He, C.-Z. Chang, C.-L. Song, L.-L. Wang, X. Chen, J.-F. Jia, Z. Fang, X. Dai, W.-Y. Shan *et al.*, Crossover of the three-dimensional topological insulator Bi$_2$Se$_3$ to the two-dimensional limit, Nat. Phys. **6**, 584 (2010).

[38] J. M. Marmolejo-Tejada, K. Dolui, P. Lazic, P. H. Chang, S. Smidstrup, D. Stradi, K. Stokbro, and B. K. Nikolic, Proximity band structure and spin textures on both sides of topological-insulator/ferromagnetic-metal interface and their charge transport probes, Nano Lett. **17**, 5626 (2017).

[39] Y. Li, F. Zeng, Steven S.-L. Zhang, H. Shin, H. Saglam, V. Karakas, O. Ozatay, J. E. Pearson, O. G. Heinonen, Y. Wu *et al.*, Giant anisotropy of Gilbert damping in epitaxial CoFe films, Phys. Rev. Lett. **122**, 117203 (2019).

[40] V. M. Edelstein, Spin polarization of conduction electrons induced by electric current in two-dimensional asymmetric electron systems, Solid State Commun. **73**, 233 (1990).

[41] K. Ando and E. Saitoh, Observation of the inverse spin Hall effect in silicon, Nat. Commun. **3**, 629 (2012).

[42] O. Mosendz, V. Vlaminck, J. E. Pearson, F. Y. Fradin, G. E. W. Bauer, S. D. Bader, and A. Hoffmann, Detection and quantification of inverse spin Hall effect from spin pumping in permalloy/normal metal bilayers, Phys. Rev. B **82**, 214403 (2010).

[43] H. Suhl, Ferromagnetic resonance in nickel ferrite between one and two kilomegacycles, Phys. Rev. **97**, 555 (1955).

[44] S.-J. Wang, D. Venkateshvaran, M. R. Mahani, U. Chopra, E. R. McNellis, R. Di Pietro, S. Schott, A. Wittmann, G. Schweicher, M. Cubukcu *et al.*, Long spin diffusion lengths in doped conjugated polymers due to enhanced exchange coupling, Nat. Electron. **2**, 98 (2019).

[45] R. Sun, S. Yang, X. Yang, A. Kumar, E. Vetter, W. Xue, Y. Li, N. Li, Y. Li, S. Zhang *et al.*, Visualizing tailored spin phenomena in a reduced-dimensional topological superlattice, Adv. Mater. **32**, e2005315 (2020).

[46] E. Lesne, Y. Fu, S. Oyarzun, J. C. Rojas-Sanchez, D. C. Vaz, H. Naganuma, G. Sicoli, J. P. Attane, M. Jamet, E. Jacquet *et al.*, Highly efficient and tunable spin-to-charge conversion through Rashba coupling at oxide interfaces, Nat. Mater. **15**, 1261 (2016).

[47] R. Liu, K. Gupta, Z. Yuan, and P. J. Kelly, Calculating the spin memory loss at Cu|metal interfaces from first principles, Phys. Rev. B **106**, 014401 (2022).

[48] J.-C. Rojas-Sánchez, N. Reyren, P. Laczkowski, W. Savero, J.-P. Attané, C. Deranlot, M. Jamet, J.-M. George, L. Vila, and H. Jaffrès, Spin pumping and inverse spin Hall effect in platinum: The essential role of spin-memory loss at metallic interfaces, Phys. Rev. Lett. **112**, 106602 (2014).

[49] S. Lee, H. Koike, M. Goto, S. Miwa, Y. Suzuki, N. Yamashita, R. Ohshima, E. Shigematsu, Y. Ando, and M. Shiraishi, Synthetic Rashba spin-orbit system using a silicon metal-oxide semiconductor, Nat. Mater. **20**, 1228 (2021).

[50] B. Zimmermann, P. Mavropoulos, S. Heers, N. H. Long, S. Blügel, and Y. Mokrousov, Anisotropy of spin relaxation in metals, Phys. Rev. Lett. **109**, 236603 (2012).

[51] X. Yang, L. Qiu, Y. Li, H. P. Xue, J. N. Liu, R. Sun, Q. L. Yang, X. S. Gai, Y. S. Wei, A. H. Comstock *et al.*, Anisotropic nonlocal damping in ferromagnet/α-GeTe bilayers enabled by splitting energy bands, Phys. Rev. Lett. **131**, 186703 (2023).